**Article:**
Unwin, AP, Hine, PJ, Ward, IM et al. (3 more authors) (2018) Novel phase separated multi-phase materials combining high viscoelastic loss and high stiffness. Composites Science and Technology, 167. pp. 106-114. ISSN 0266-3538

https://doi.org/10.1016/j.compscitech.2018.07.032

# Novel phase separated multi-phase materials combining high viscoelastic loss and high stiffness

A.P.Unwin[1], P.J.Hine[1], I.M.Ward[1], M.Fujita[2], E.Tanaka[2] and A.A.Gusev[3]

1- Soft Matter Group, School of Physics and Astronomy, University of Leeds, Leeds, LS2 9JT, UK

2 - The Kaiteki Institute, Mitsubishi Chemical Holdings,

1-1 Marunouchi 1-chome, Chiyoda-ku, Tokyo, Japan

3 - Institute of Polymers, Department of Materials, ETH Zürich, 8093 Zürich, Switzerland

Abstract

In a previous study we showed that a unique combination of high stiffness and high viscoelastic loss could be achieved by filling a polystyrene matrix with rigid inorganic spheres coated with a thin (~200nm) layer of a viscoelastic material. The sandwiching of this 'lossy' layer between the two rigid components was found to give a significant amplification of the tanδ loss peak associated with this material, without significantly compromising the sample stiffness. This was an experimental validation of the effect originally proposed by Gusev using finite element numerical studies. Following on from this, in the current study we have developed this concept further and shown that a similar amplification of viscoelastic loss can be achieved by incorporating rigid, but uncoated, particles into a phase separated matrix blend of polystyrene (PS) and a polystyrene/polyisoprene/polystyrene triblock co-polymer (SIS). The inspiration for this choice of the PS/SIS blend as the matrix came from some previous work where we studied, and modelled, the viscoelastic properties of these materials. In this work we show that in the filled PS/SIS blends, the loss amplification effect can been seen for different PS/SIS ratios, for different SIS polymers with different glass transition temperatures and also for glass fibres as well as for spherical particles. The key to seeing this effect is the fact that the SIS rubber phase was found to form a thin coating on the surface of the embedded particles during processing, effectively producing a surface coating layer on the particles (as well as phase separating within

the PS matrix). As with our previous studies, it is shown that the experimentally measured effects are closely predicted by numerical micromechanical modelling based on the measured bulk properties of the three discrete components.

## 1 Introduction

The research into new composite materials for reducing sound and vibration levels remains a dynamic area of scientific study due to ongoing concerns of environmental noise pollution. Thus, for example, when designing new buildings, or new vehicles (for instance cars or aircraft), the level of noise that is generated or the ability to absorb noise in service is an important consideration for the designer. Access to materials that are both structural (have a reasonable stiffness) and able to absorb or damp unwanted noise or vibration is highly desirable but it is a technological challenge to develop materials that simultaneously possesses these two requirements, namely high stiffness and high dynamic loss.

One method to trade-off stiffness and damping, is to utilise a composite material where the reinforcing fibre has improved damping characteristics, such as the recent work of Rueppel et al [1]. An alternative strategy for achieving this balance between structural stiffness and loss properties is through the use of laminate systems, for example a sandwich composed of a viscoelastic 'lossy' layer between two composite stiff and elastic layers [2, 3]. Van Vuure [4] describes how this approach can help to damp out structural vibrations by exciting additional shear deformation in the constrained layer. Alvelid [5] also describes how a laminate system can help reduce the number of vibrational modes in an automotive body, and how a high loss visco-elastic layer was attached to the base structure and then capped by a stiffer outer (metal) layer. Alvelid also proposed that when the base structure was subjected to bending, high shear deformations were developed in the visco-elastic layer leading to enhanced energy absorption.

The phenomenon of enhanced energy loss in dynamic loading of composite structures has come to be referred to as loss amplification.

Kristensen [6], following on from earlier theoretical studies by, for example, Kerwin [7] and Wang [8] has explored the phenomenon of loss amplification using modelling. Using a combination of simple beam theory and a full 2D finite element model he was able to demonstrate loss amplification in composite beams and show how the addition of a stiff outer constraining layer led to enhanced damping of the structure by forcing large shear strain deformations into the constrained visco-elastic layer, thereby confirming the proposal of Alvelid. Other authors have used intricate finite element simulations to explore the phenomenon and shown that the damping properties of sandwich structures can be optimised using either continuous [9] or discrete visco-elastic layers added as patches onto a composite structure [10].

A key parameter to emerge from these theoretical studies is the thickness of the visco-elastic layer. In a further theoretical paper, Gusev [11] showed that for a laminate morphology composed of two layers (a stiff, non lossy layer and a weak, lossy layer) the effective loss modulus of the combination passed through a peak at a volume fraction of the lossy layer of ~0.001. Intriguingly, the loss amplification was very large, with the loss modulus of the combination being around 300 times larger than the value for the individual viscoelastic layer.

While these loss amplification effects in laminate composites are very interesting and currently used commercially, there is a significant limitation as laminate structures can be inappropriate for manufacturing parts with non-simple shapes . Gusev [11, 12] offered an alternative to the multi-layer laminate approach, based on the incorporation of coated spherical inclusions. A combination of finite element studies and analytical modelling approaches showed that significant amplification of the loss properties could be achieved by coating each particle with

a thin, and lossy, visco-elastic layer. These results mirrored those for the laminate beams, but offered a material in which the amplified lossy behaviour was isotropic and which also could be processed into a complex final shape using, for example, injection moulding. In a recent study [13] , we proved that such materials could be experimentally realised by embedding coated glass spheres into a polystyrene matrix, and that the loss amplification effects produced were in close agreement to those predicted micromechanically.

In this current work we have further developed this idea by utilising and combining a number of existing concepts from the polymer blend literature [14, 15]. In a recent paper [16], we investigated the properties of a range of blends of polystyrene (PS) and a polystyrene/polyisoprene/polystyrene (SIS) triblock thermoplastic rubber copolymer using a combination of experimental and numerical approaches. The two components were found to phase separate during processing. But most importantly, as is found in this current work, on incorporation of a rigid particle (either spheres or fibres) a thin layer of the SIS copolymer is seen to form on the surface of the particles, see Fig. 1, effectively producing a coated particle as investigated and described in our previous work [13].

Four main systems were fabricated and studied in this work and were as follows: spherical Barium titanate beads in a 90/10 PS/SIS (glass transition temperature Tg 10°C) matrix; spherical Barium titanate beads in an 80/20 PS/SIS (Tg 10°C) matrix; spherical Barium titanate beads in a 90/10 PS/SIS (Tg -15°C) matrix; glass fibres in a 90/10 PS/SIS (Tg 10°C) matrix.

## 2 Experimental

### 2.1 Materials

All the composite samples investigated here have been produced using a combination of three components, namely a polystyrene, a triblock rubber and a rigid glass filler. The polystyrene

was a commercially available, grade BASF PS2, with a weight-average molecular weight (Mw) of 274 000 g/mol and a polydispersity of 2.74. The triblock thermoplastic Hybrar rubbers had the chemical structure polystyrene/polyisoprene/polystyrene (SIS) and were obtained from Kuraray Co Ltd. The symmetric SIS triblocks had a total fraction of polystyrene in the end blocks of 20%.

Two Hybrar grades were chosen that had glass transition temperatures (Tg) significantly lower than that of the PS grade (108°C), with which they would be blended. Our previous research [16] showed that this PS/SIS combination formed phase separated blends. The two grades were 5127 with a Tg of 10°C and 7125 with a Tg of -15°C: for the remainder of this paper these will be designated as high Tg and low Tg.

Two forms of rigid fillers were used in this study, in the form of glass spheres and glass fibres. The spherical glass spheres, grade UB-02M, were obtained from Unitika, Ltd. and were selected for the narrowness of its size distribution, but mainly to retain consistency with previous studies where they were used in a coated form [13]. The beads were made from a Barium titanate glass with a density of 4.2 $gcm^{-3}$ and had an average diameter, measured using a standard particle sizer, of 42μm. The glass fibres (E glass) were supplied by Asahi Fiber Glass Co. Ltd and had a diameter of 10μm and an average aspect ratio of 20.

## 2.2 Sample manufacture

### 2.2.1 Production of the composite blends

Two stages were involved in the preparation of the composite samples, namely preparation of the matrix (PS/SIS blends) and subsequent incorporation of the fillers into these blends. Both of these stages were carried out using a Europrism twin screw extruder set to a temperature of 220°C.

The matrix for all the composite samples considered here was a blend of the PS and the SIS triblock, so these materials needed to be blended as a prerequisite to composite production. A premix, at the desired PS/SIS ratio, was first produced by weighing pellets from the two components. These hand mixed pellets were then introduced at the start of the extruder using a controlled speed feeder. The blended extrudate was passed directly into a water bath and then immediately chopped into pellets. Two blend ratios of PS/SIS were prepared, namely 90/10 and 80/20 by volume. As described in a previous publication [16], these blends were phase separated comprising distinct zones of the SIS rubber within the PS matrix as also previously reported by Matsuo [17].

The second stage was to blend the particles into the chosen matrix. For this stage, the blended extrudate pellets of the matrix were reintroduced at the start of the extruder barrel while the particles were introduced between the second and third mixing zones using a controlled feed from a second hopper. The mass feed rates of the two hoppers were first calibrated, so a range of mass fractions of the final composite could be achieved. Particle volume fractions between 0 and 40% were prepared for the various blends. Final particle fractions were determined by measuring the sample densities and knowing the densities of the various phases. Table 1 shows the four different composite systems that were investigated.

| Sample designation | SIS grade and Tg | PS/SIS ratio | Filler type | Filler Volume fractions (%) |
|---|---|---|---|---|
| 1 | 5127 10°C | 90/10 | Spheres | 18, 33, 39, 44 |
| 2 | 5127 10°C | 80/20 | Spheres | 20, 32, 41, 45 |
| 3 | 7125 -15°C | 90/10 | Spheres | 19, 28, 41, 49 |
| 4 | 5127 10°C | 90/10 | Fibres | 34 |

Table 1: Different composite systems investigated in this study

2.2.2 Preparation of samples for the viscoelastic testing

Pellets of the blended composites were placed between brass plates in a hot press set at a temperature of 180° C and then pressed for four minutes before slow cooling to room temperature under pressure. Spacers were placed between the brass plates to achieve the required specimen thickness for the subsequent tests.

### 2.3 Dynamic mechanical thermal analysis (DMTA)

The viscoelastic tests were carried out in rectangular torsion using a Rheometrics Dynamic Spectrometer RDS II. Samples of the required dimensions (10mm wide, 1.4mm thick and 55mm long) were cut from the compression moulded sheets. Samples were tested over a range of temperatures (between -40 and +70°C) at a frequency of 1Hz and an oscillatory strain of 0.05%.

### 2.4 Morphology SEM

The morphology of the multi-phase blends was studied using scanning electron microscopy (SEM) and transmission electron microscopy (TEM). For the SEM micrographs, the samples were prepared in two different ways. The chosen surfaces were first prepared using a cross section polisher (JEOL Ltd Model SM-09010), which irradiates the sample with an argon beam inside a vacuum chamber and produces a flat surface for examination without the plastic deformation often seen in other preparation techniques (for example freeze fracture). Then for the first technique (which worked best for the glass bead composites), the flat surfaces were subjected to ion-beam milling, which preferentially etched away the softer (rubber) component to give contrast in terms of surface height. In the second technique (which worked better for the glass fibre composites), the flat surfaces were stained with osmium tetroxide. The dispersed rubber phase was then preferentially stained darker by this technique, also giving contrast between the various phases. The TEM studies were carried out using a JEM-1230 (JOEL Ltd.). The

prepared microtomed slices were stained with osmium tetroxide. The dispersed rubber phase was preferentially stained darker by this technique.

## 3 Results

### 3.1 Morphology

Figure 1 shows a number of SEM and TEM micrographs from the various composite blends to illustrate the composite morphology at different length scales. Figure 1a is a low magnification SEM picture of a sample incorporating spherical particles, showing that the particles are well dispersed. Figure 1b is a higher magnification (stained) TEM micrograph of a matrix region from a 90/10 PS/SIS blend. Here, the phase separated SIS rubber zones can be clearly seen, which in this region have been elongated during processing. In the DMTA results that are presented in the following sections, these distinct SIS zones within the PS matrix are associated with the glass transition temperature of the pure SIS component (as seen in our previously published PS/SIS study [16]). Figure 1c shows a high magnification stained TEM and shows clearly the presence of a precipitated layer of the SIS rubber on the particle surface, as well as phase separated rubber zones within the PS matrix as shown on Figure 1b. Most interestingly, for interpreting the experimental results of this study, is the variable thickness of the interfacial rubber layer on the surface of the beads. Finally, Figure 1d shows a stained SEM picture for a glass fibre PS/SIS blend. Again there are darker regions within the PS matrix which can be associated with the phase separated SIS component. However, and equally important, Figure 1d again shows evidence for a darker SIS rubber layer on the glass fibre surfaces, which in some cases is connected to some of the SIS regions within the PS matrix. Figures 1c and 1d lead us to conclude that a thin layer of the SIS rubber component has by good fortune, precipitated on the surfaces of the embedded particles (both for glass beads and

glass fibres) during melt processing and cooling, hence forming a thin coating layer. The proposal is that this thin precipitated layer is responsible for the second, and highly amplified, peak, seen in the following DMTA tanδ results. This will also be corroborated by numerical modelling results presented in section 4.

### 3.2 Dynamic temperature results

#### 3.2.1 Spherical Barium titante beads in a PS/SIS (High Tg) 90/10 blend

Figure 2 shows the DMTA torsion results for a 90/10 PS/SIS blend filled with a range of spherical bead fractions. In terms of tanδ, which shows the most interesting results, all four glass bead fractions showed a small peak at a temperature associated with the Tg of the SIS component (~10°C). Interestingly, the height of this peak did not change as the volume fraction of the glass beads was increased. The emergence of the second peak at a higher temperature (~30°C) in the composite samples is striking and is seen to be very dependent on the volume fraction of filler, reaching a maximum value of 0.14 for the highest bead fraction of 44%. The corresponding modulus is approximately 2.5GPa so this combination had both a higher modulus (x2) and significantly higher tanδ (x14) compared to pure polystyrene. This combination of increased stiffness and loss is a rare combination.

#### 3.2.2 Spherical barium titante beads in a PS/SIS (High Tg) 80/20 blend

These striking results were also seen in composites using the 80/20 PS/triblock blend as the matrix (Figure 3). Again the composite samples showed two distinct tanδ peaks at similar temperatures to those observed in the composites based on the 90/10 PS/triblock matrix. The height of the lower temperature peak is seen to be almost twice as high than for the 90/10 blend, confirming that this due to the SIS component and mirroring the results from our

previous study on PS/SIS blends [16]. Again the amplitude of this lower peak is practically independent of the glass bead volume fractions, while the higher temperature peak is very dependent on the filler fraction (cf. Figure 2). Interestingly, the magnitude of the upper peaks at the various particle fractions is similar to that seen for the 90/10 blend (~0.14) suggesting that the height of the amplified peak correlates with the percentage of glass beads (or their surface area), rather than with the fraction of the PS/SIS/PS triblock. In this case, a lower SIS fraction would seem a more practical option, as the additional SIS component leads to a fall in the stiffness of the sample. We suspect that once there is enough of the SIS rubber to precipitate on the surfaces of the embedded particles, then adding further SIS rubber is counter-productive as it leads to a larger decrease in the storage modulus without any benefit in loss amplification. We also found that for a 70/30 blend (which we did manufacture but not reported here), the SIS rubber zones become conjoined and that the storage modulus was quite low. It is quite possible that an even lower fraction of SIS than 10% might be optimum, but that was not studied in this work.

### 3.2.3 Spherical Barium titanate beads in a PS/SIS (Low Tg) 90/10 blend

Figure 4 shows the DMTA torsion results for a 90/10 PS/SIS blend filled with a range of spherical bead fractions but this time for the SIS blend with a lower Tg of -15°C rather than +10°C as shown in Figure 2 and 3. In essence the results are almost identical to those for the higher Tg SIS component shown in Figure 2, but just shifted down by ~25°C, which is close to the difference in Tg of the two SIS grades. As seen before, the height of the lower peak associated with the SIS component is independent of the fraction of glass beads and is at the position associated with the Tg of the pure SIS materials, while the upper peak (which is again ~30°C higher than the lower peak) increases significantly as the particle fraction is increased. The maximum amplitude of ~0.14 for tanδ is very comparable to the other two materials so far

investigated. The use of the lower Tg SIS component results in the peak in tanδ (maximum loss) being just below room temperature, showing that this effect can be achieved at a particular temperature by changing the nature of the viscoelastic component.

### 3.2.4 Glass fibres in a PS/SIS (High Tg) 90/10 blend

The final system to be studied mixed short glass fibres (with an average aspect ratio of 20) into a matrix of the PS/SIS (High Tg) 90/10 blend and the results, for just one fibre volume fraction of 34%, are shown in Figure 5. It is seen that the results for the glass fibres mirror those shown previously for the spherical particles in Figure 2, suggesting strongly that the loss amplification effect can achieved using either spheres or fibers. There is obviously another layer of complexity when using fibres as the rigid filler, as they are likely to have both a polydispersed length distribution together with an orientation distribution. While these aspects are outside the current study, it is clear that the enhanced loss amplification peak can be achieved using glass fibres, offering the possibility of achieving this behaviour in standard injection moulding fibre reinforced polymer grades.

## 4 Numerical Modelling

The results in Figures 2-5 exemplify that the proposed loss amplification effect can be experimentally achieved. For further optimisation of the balance of stiffness and loss, it would be advantageous to have validated numerical models, as this would allow more rapid design of the important variables (Tg of the viscoelastic component, particle shape and fraction, etc) to be more easily investigated rather than have to manufacture and test each composite.

In a previous published study, Gusev [12] used finite element techniques to validate a purely analytical approach for predicting the viscoelastic properties of coated spherical particle composites. It was shown that the ‘n-layered’, or composite sphere micromechanical model,

analytically solved by Herve and Zaoui [18], could provide almost identical results to a finite element approach but with a fraction of the numerical effort required. The study also made use of the elastic-viscoelastic correspondence principle where the elastic modulus is replaced by a complex form incorporating both elastic and loss components.

In the current study we have used the conclusions of this previous work and have used the 'n-layered' micromechanical model to produce numerical predictions of the storage shear modulus and tanδ of appropriate idealised composite microstructures in an effort to gain insight into the relationship between the morphology and mechanical behaviour of our samples. This strategy is strengthened by another recent study [13], where we showed excellent predictions of the experimental behaviour using the same Barium titanate beads used here, but spray coated with a different viscoelastic polymer and then incorporated in the same polystyrene matrix [13]. In that study, very close agreement was found between the experimental measurements and the numerical micromechanical predictions, giving us confidence to follow the same strategy with the materials in this study.

Figure 6 shows the details of the micromechanical model, which comprises three concentric spheres embedded in a fourth material (phase n=4), which is an effective homogeneous medium which will have the properties of the composite once they are determined. The inner sphere, with radius $R_1$, is the rigid reinforcing particle. Next, the shell between radii $R_2$ and $R_1$ is the coating layer. Finally the shell between radii $R_3$ and $R_2$ corresponds to the polystyrene matrix. The values of $R_1$, $R_2$ and $R_3$ are varied in order to achieve the desired ratios of the three components determined for the various experimental materials and perfect bonding is assumed at all interfaces. Isotropic homogeneous linear elastic phases are also assumed. For solving, the medium is subject to uniform strains at infinity and the displacement and stress continuity equations at interfaces are solved using the generalized self-consistent Christensen-Lo energy

approach [19] , i.e., by requiring that the average strain energy density stored in the multi-layered inclusion be the same as in the effective medium at infinity.

To determine the effective shear modulus, a simple shear is applied at infinity. In a spherical coordinate system $(r,\theta,\phi)$ with its origin at the common spheres' centres (see Figure 6), the fundamental (homogeneous) solutions of the Lamé-Navier equilibrium equations for the displacement vector $\mathbf{u}=(u_r,u_\theta,u_\phi)$ are known from Love [20], Goodier [21], Matonis [22] and Wang and Schonhor [23] and they are given by

$$u_r^{(i)}=\left(A_i r-\frac{6\nu_i}{1-2\nu_i}B_i r^3+\frac{3C_i}{r^4}+\frac{5-4\nu_i}{1-2\nu_i}\frac{D_i}{r^2}\right)\sin^2\theta\cos 2\phi \tag{1}$$

$$u_\theta^{(i)}=-u_\phi^{(i)}=\left(A_i r-\frac{7-4\nu_i}{1-2\nu_i}B_i r^3-\frac{2C_i}{r^4}+\frac{2D_i}{r^2}\right)\sin\theta\cos\theta\cos 2\phi \tag{2}$$

where r is the distance from the origin, $\theta$ and $\phi$ are the two spherical angles, $\nu_i$ Poisson's ratio of phase i, and $A_i$, $B_i$, $C_i$ and $D_i$ are the undetermined coefficients. To avoid singularity at the origin, coefficients $C_1$ and $D_1$ must vanish while $B_4$ must vanish to avoid divergence at infinity. Coefficient $A_4$ is related to the simple strain $\gamma$ at infinity as $A_4=\gamma$. Coefficient $D_4$ is obtained using the Chistensen-Lo's energy condition [19]. This gives $D_4=0$. The remaining eleven unknown coefficients plus the yet unknown effective shear modulus are determined by satisfying the twelve independent displacement and stress continuity conditions at the three interfaces, see Figure 6.

The effective shear modulus G is then given by the positive root of the following second order equation

$$a\left(G/G_m\right)^2+b\left(G/G_m\right)+c=0 \tag{3}$$

where $G_m$ is the matrix shear modulus and a, b and c are the coefficients given by rather cumbersome but nonetheless closed-form arithmetic expressions involving as input parameters the elastic moduli and the volume fractions of the matrix, interface and inclusion phases, see Section III(b) of Hervé and Zaoui [18].

Since solution (3) is in analytical form, the elastic-viscoelastic correspondence principle is used to convert this static solution to steady-state harmonic solution simply by replacing static phase bulk and shear moduli $K_i$ and $G_i$, respectively, by the complex viscoelastic moduli $K_i^*(\omega)$ and $G_i^*(\omega)$ at a given angular oscillation frequency $\omega$ (Hashin, [24]; Christensen [25], Gusev, [12]). Mathematica 9.0 (www.wolfram.com) was used to implement and solve the model's complex arithmetic equations. For a single evaluation of the effective shear modulus, the solution time was some tenth of a second on a typical Intel Pentium i7 processor.

A key aspect for any modelling is the input parameters, which here are the viscoelastic properties of the three components. For the Barium titanate reinforcing beads the average diameter was 42μm; and the bulk modulus (142 GPa) and shear modulus (47 GPa) were taken from [26]. For the high Tg Hybrar rubber and the polystyrene matrix, the viscoelastic properties have already been measured as a function of temperature by the authors in a previous paper investigating the properties of blends of these two materials [16]. Figures 3 and 4 in this previous reference show the properties of the PS and SIS rubber components.

The simulations also require the bulk modulus of the different viscoelastic components and this is known to be lossy and temperature dependent across the glass transition region [27]. In the absence of experimental measurements it has been assumed that the bulk modulus is purely elastic, temperature invariant and has a value of 4GPa. This is a reasonable assumption, as a previous study by Gusev [12] showed that introducing a lossy component for the bulk modulus

for coated spheres gave almost indistinguishable results from those obtained using a purely elastic form. This strategy can be considered validated by the success of the predictions for coated Barium titanate beads described in [13].

Figure 7 shows a comparison between the predictions from the numerical model for a range of particles fractions in the PS/SIS (high Tg) 90/10 blend, based on an average estimate of an SIS layer thickness around each particle of 200nm, chosen based on the SEM pictures. The numerical results show noise as they are based on real experimental torsion measurements from samples of the pure SIS rubber and unfilled PS/SIS blends [16]. It is clear the model, which considers only micromechanical effect, captures the essence of the experimental results very well. In particular the amplitude of the loss amplification peak (the higher temperature peak) is very well predicted. However there are some interesting differences between the experimental results and predictions, which can be seen more clearly in Figure 8, which shows a direct comparison of the experimental measurements and numerical predictions for only the highest particle fraction of 44%. The Figure shows that the storage modulus above and below the glass transition of the SIS high Tg rubber is well predicted, but that the transition for the experimental measurements is more gradual than predicted. Similarly, while the amplitude of the loss peak in tanδ is in good agreement, the temperature of the amplified peak is seen to be predicted to be at a lower temperature (~10°C) to that measured experimentally and the peak also is predicted to be much narrower. This is an intriguing result, as the previous study on directly coated particle systems showed much closer agreement [13] . There are a number of possible reason for this interesting divergence. First, as seen from the SEM pictures and in particular Figure 1d, the precipitated SIS layer is not always of a constant thickness (as was achieved with the previously reported direct spraying method), and this would have the effect of broadening the transition. Second, while the spray coating used in the previous study was amorphous, the SIS rubber itself forms phase separated structures within the SIS zones (see

Figure 1d here and Figure 2 in the previous work on only the PS/SIS blend [16]), so this could produce some very interesting structures around the Barium titanate beads with different properties to the bulk. These aspects were outside of the current study but would be of interest for future work.

For the other spherical particle composites, a similar pattern was seen for both the 80/20 PS/SIS (High Tg) blend as the matrix and the 90/10 PS/SIS (Low Tg) as the matrix. For predicting the properties of the short fibre composite, this is a much more detailed proposition, as it requires finite element predictions, as there is currently no available analytical model for coated cylindrical particles (which also requires orientation averaging to produce the final predictions). This two-step finite element viscoelastic homogenization procedure has been used in our recent work on uncoated short fibre composites [28] but is outside the scope of the current paper to achieve this for coated fibres.

## 5 Discussion

There are two main strands to the work presented here. The first shows, from experimental measurements, that composites made from uncoated glass spheres or fibres in a PS/SIS matrix can display a significant loss amplification effect. This effect by itself is not novel as laminate structures also show the effect (for example [4, 5]) but unlike the laminate structures these materials are isotropic and do not require special structural construction so they are suitable for conventional production methods such as injection moulding. Furthermore, the lack of critical sensitivity to matrix composition and the nature of the filler content suggests that control of any manufacturing process would not be difficult to achieve. The second strand relates to micro-mechanical modelling using the n-layered model [17] to investigate the mechanical behaviour of specific model structures.

Many authors [4-6, 11, 12] have shown that the amplification of the viscoelastic loss of a thin constrained rubber layer (over a bulk measurement) is due to the development of very high shear strains in this layer. Simulations investigating the effect of changing the thickness of this layer have shown that if the layer is too thin, then sufficient material is not involved, whereas if the layer is too thick the constraint effect is not significantly enhanced [13]. For the Barium titanate beads used in this work, a layer thickness of the order of a few hundred nanometres would appear to be optimum (giving maximum amplification without significant stiffness loss). Fortuitously, this is the range of thickness of precipitated rubber layers developed in the materials produced for this study.

It is of interest to assess the combination of stiffness and damping achieved in these materials against other materials. In a previous study [13], we compared such properties against the commonly used Ashby Materials Selection chart for tanδ (which Ashby terms η) versus the storage Young's modulus E' (simply termed E in the chart) [29, 30]. This chart (shown as the background in Figure 9), indicates that there is usually a trade-off between viscoelastic loss coefficient and storage modulus, with materials clustering around a dashed line where the product of these two quantities is given by, $\eta E = 0.04$ GPa. In this study we have measured the viscoelastic torsion modulus, G, and so to produce a value for plotting on the Ashby Loss Coefficient chart we have used the normal approximation of $E \sim 3G$. The 'best' result from this study, for a PS/SIS 90/10 matrix incorporating 44% spherical particles, has also been added to this design chart, and is seen to lie significantly above this dashed line, with a value of the product, $\eta E = 1.1$ GPa, which is an increase of well over an order of magnitude, validating the aim of producing materials with an increased stiffness and damping.

## 6 Conclusions

In this study we have used a combination of experimental measurements and numerical methods to investigate the unusual viscoelastic behaviour of a range of multiphase composite materials, which incorporate rigid particles into a phase separated matrix blend of polystyrene and polystyrene/polyisoprene/polystyrene triblock co-polymer. DMTA torsion measurements showed that these materials displayed a novel combination of high shear stiffness and high viscoelastic loss close to the glass transition temperature of the bulk triblock co-polymer. In particular, a second, highly amplified, peak was seen in the tanδ DMTA torsion measurements, which we attribute to a thin precipitated layer of the viscoelastic SIS component. This study has displayed a practical way to achieve such materials [31], which can prove alternatives to the normally used technique of sandwiching a thin viscoelastic layer between two stiff outer layers. While the laminate approach can be limited in terms of shape and anisotropy, the new proposed materials display this novel behaviour in all directions (isotropic) and would have the ability to be injection moulded into more intricate shapes if desired.

The study also shows how simplified pure micromechanical modelling schemes can be very helpful in understanding the key underlying physics for a particularly measured behaviour. While this does not necessarily give a perfect quantitative match with the behaviour of the real systems the agreement is striking even though it does not contain any molecular level detail (structure within the triblock blends, molecular constraint in thin layers etc) and hence such modelling will be very valuable for further design optimisation of these interesting systems.

## 6 Acknowledgements

The initial impetus for this work came from the discussions with Prof. G.H. Fredrickson of UCSB (Santa Barbara, U.S.A.).

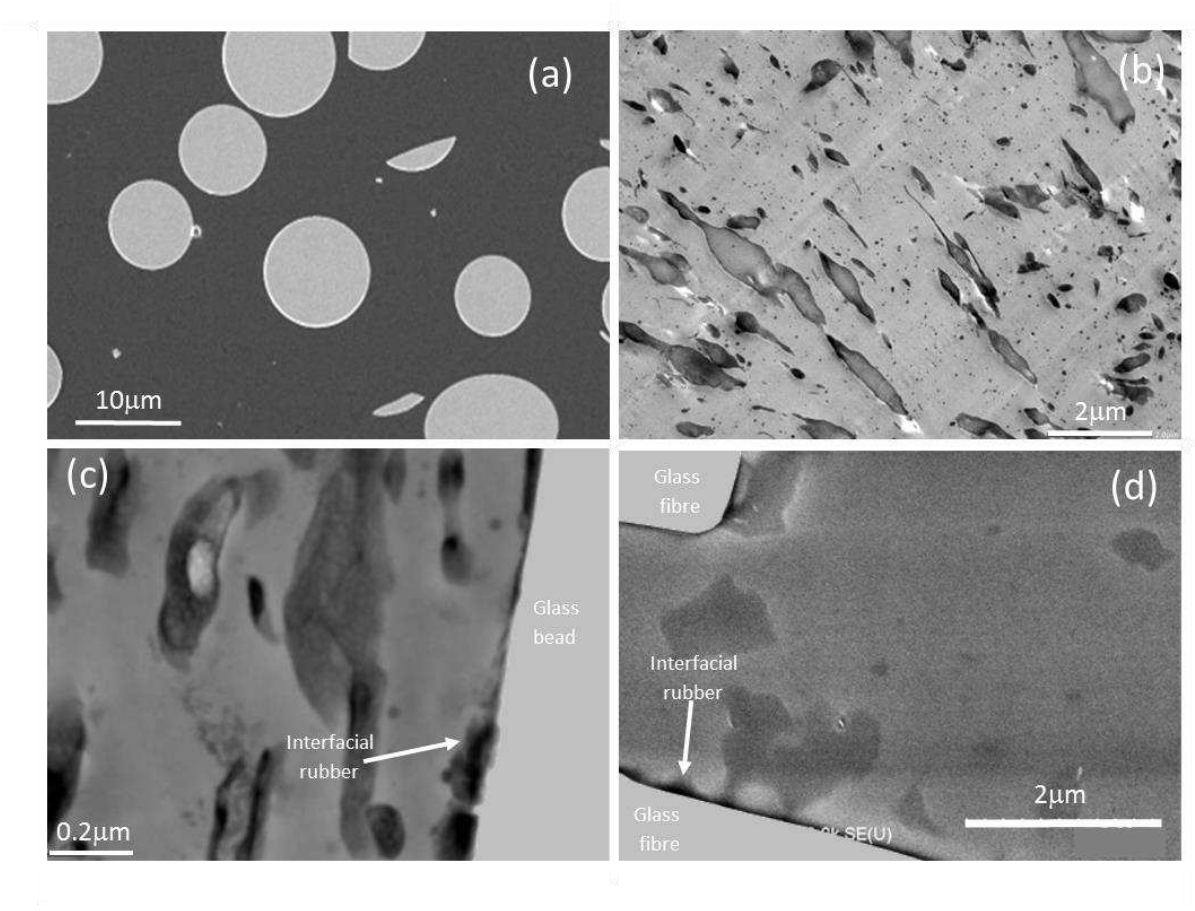


Figure 1: SEM and TEM micrographs of the filled composites showing the morphology at the various length scales.

a) Low magnification SEM image showing dispersed spherical particles. b) Stained TEM picture showing details of the phase separated SIS rubber regions in the PS matrix. c) High magnification stained TEM of the same sample as in Figure 1b with incorporated spherical particles showing structure within the phase separated SIS rubber zones, and the intermittent nature of the SIS rubber on the surface of the glass bead. d) Stained SEM 90/10 PS/SIS (high Tg) sample with incorporated glass fibres again showing the precipitated rubber layer on the glass fibre surfaces.

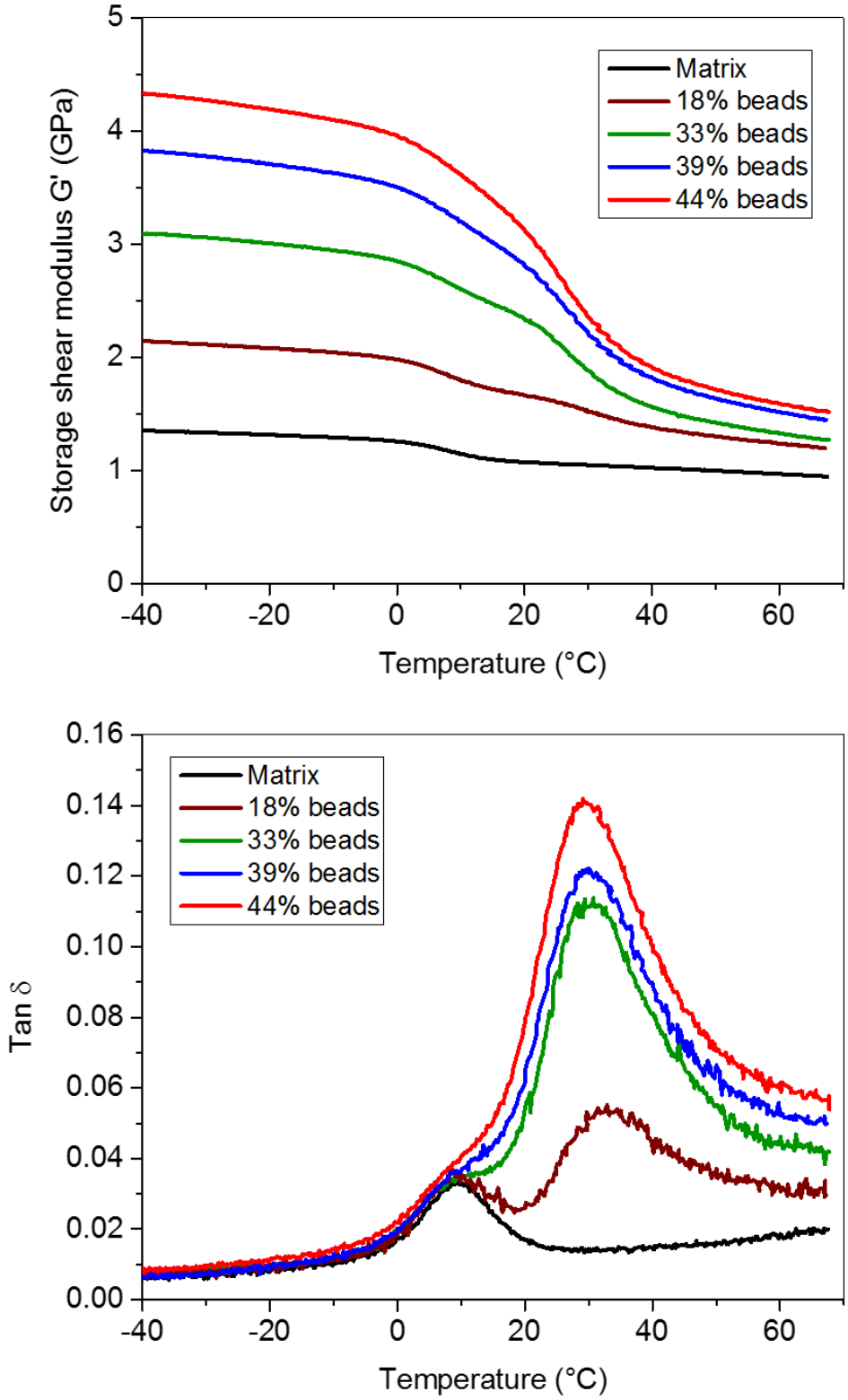


Figure 2: Storage modulus (G') and tan δ versus temperature for various fraction of Barium titanate glass beads in a PS/SIS (high Tg) 90/10 blend.

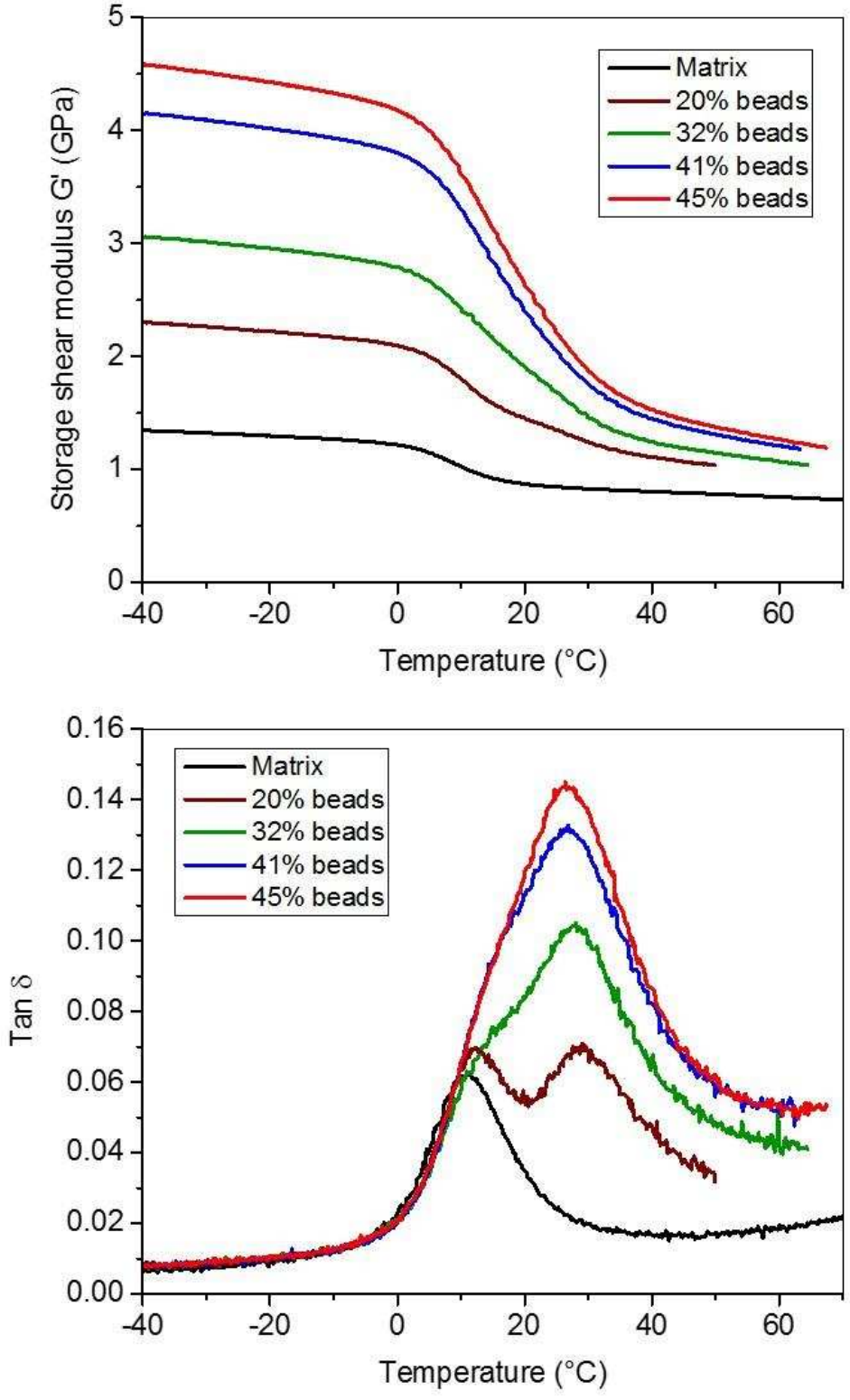


Figure 3: Storage modulus (G') and tan δ versus temperature for various fraction of Barium titanate glass beads in a PS/SIS (high Tg) 80/20 blend.

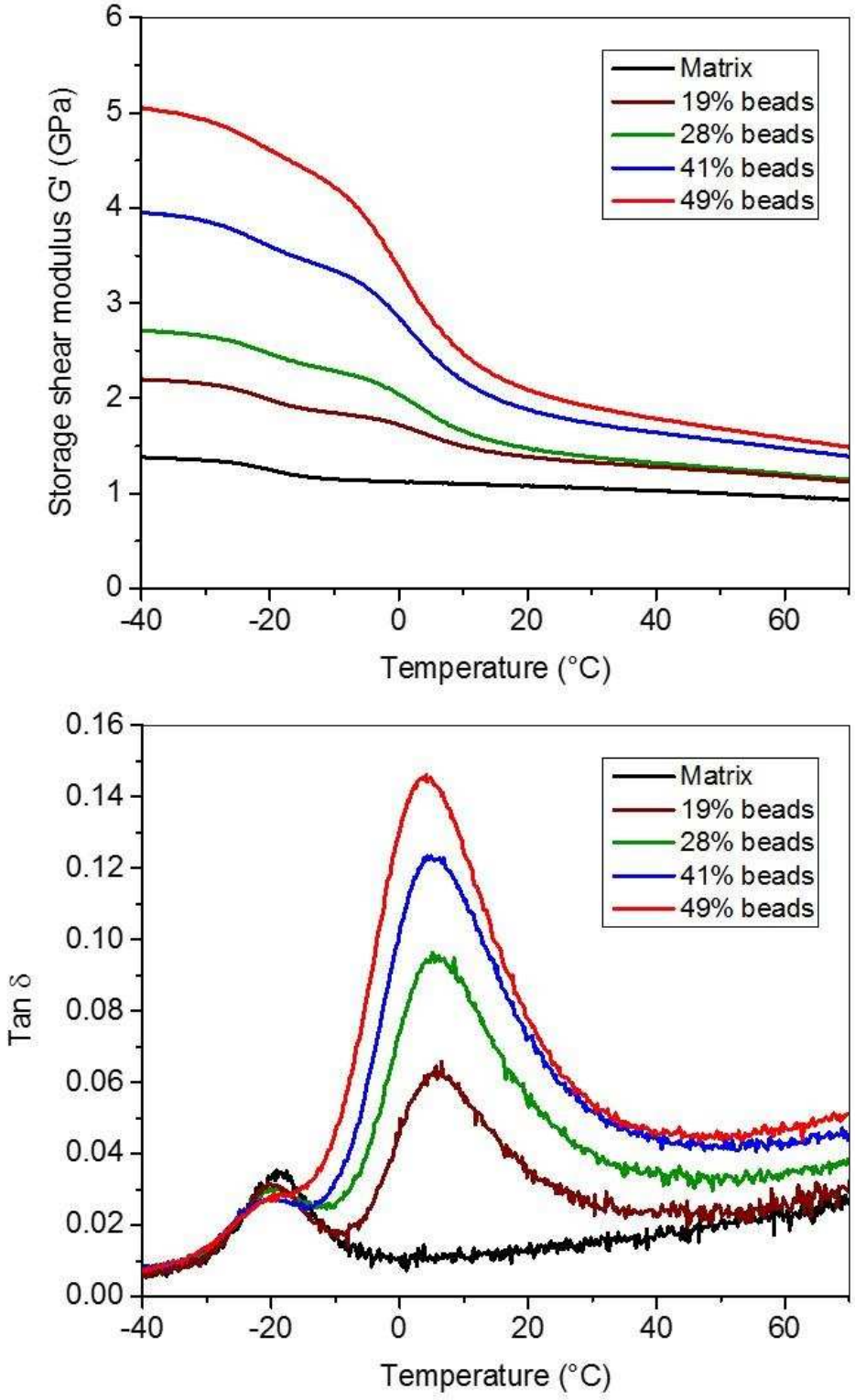


Figure 4: Storage modulus (G') and tan δ versus temperature for various fraction of Barium titanate glass beads in a PS/SIS (low Tg) 90/10 blend.

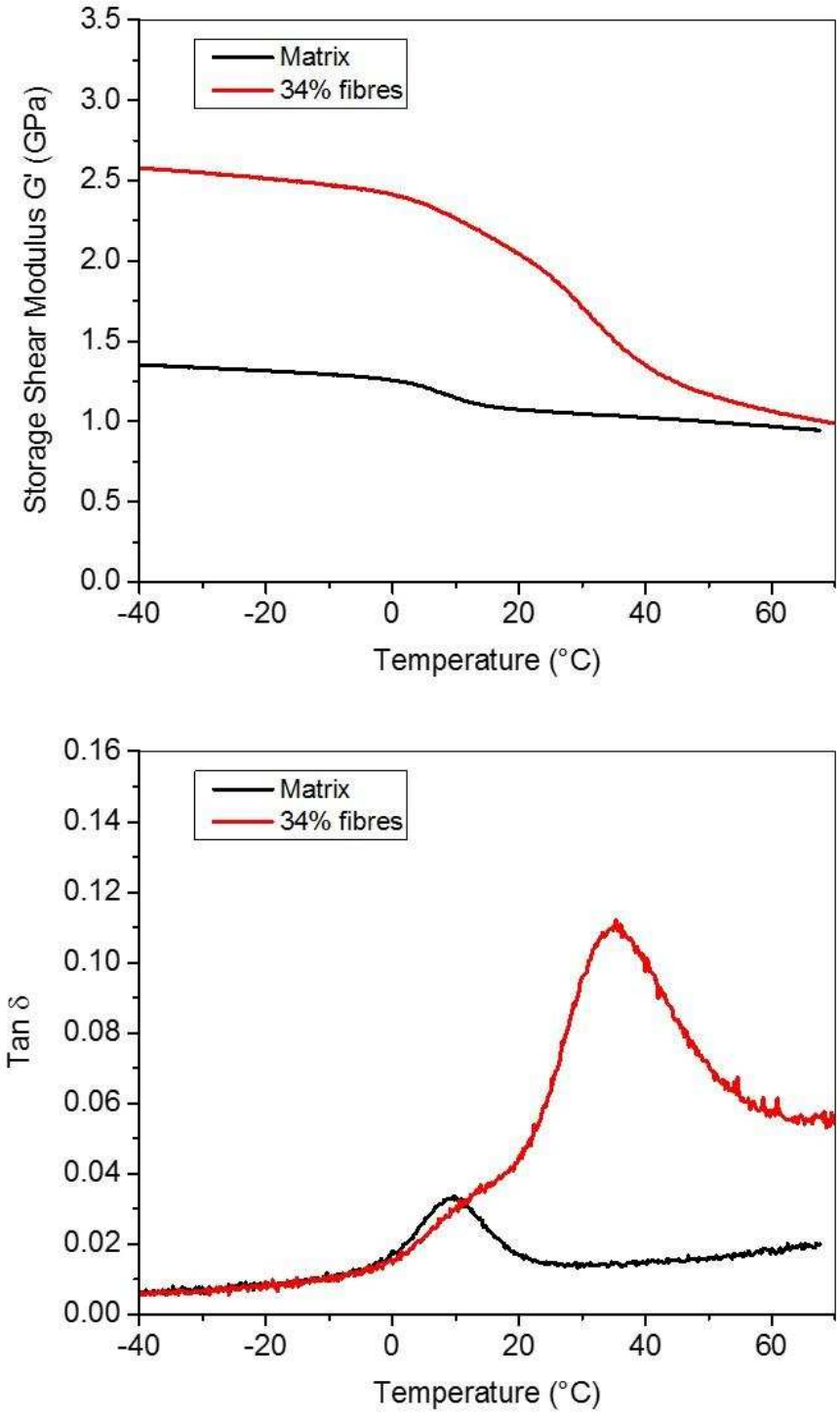


Figure 5: Storage modulus (G') and tan δ versus temperature for a volume fraction of 34% glass fibres (aspect ratio = 20) in a PS/SIS (High Tg) 90/10 blend.

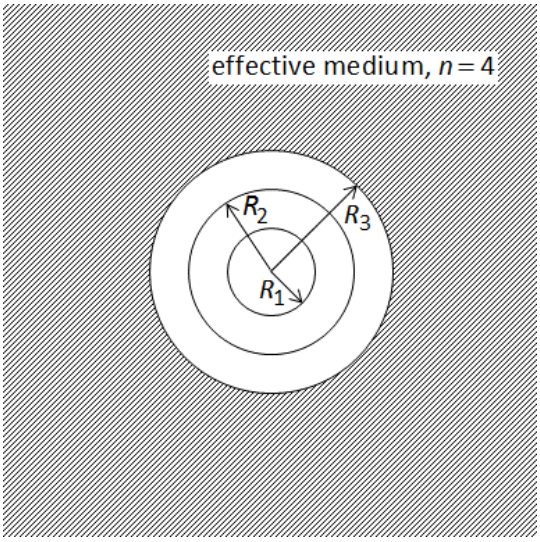


Figure 6: A representation of the n-layered model for a composite filled with coated spherical particles. The three concentric spheres have radii $R_1$, $R_2$ and $R_3$ . The inner sphere ($R_1$) is the rigid particle, the shell between $R_2$ and $R_1$ is the coating layer, while the shell between $R_3$ and $R_2$ corresponds to the polystyrene matrix. This structure is then embedded in an infinite effective medium.

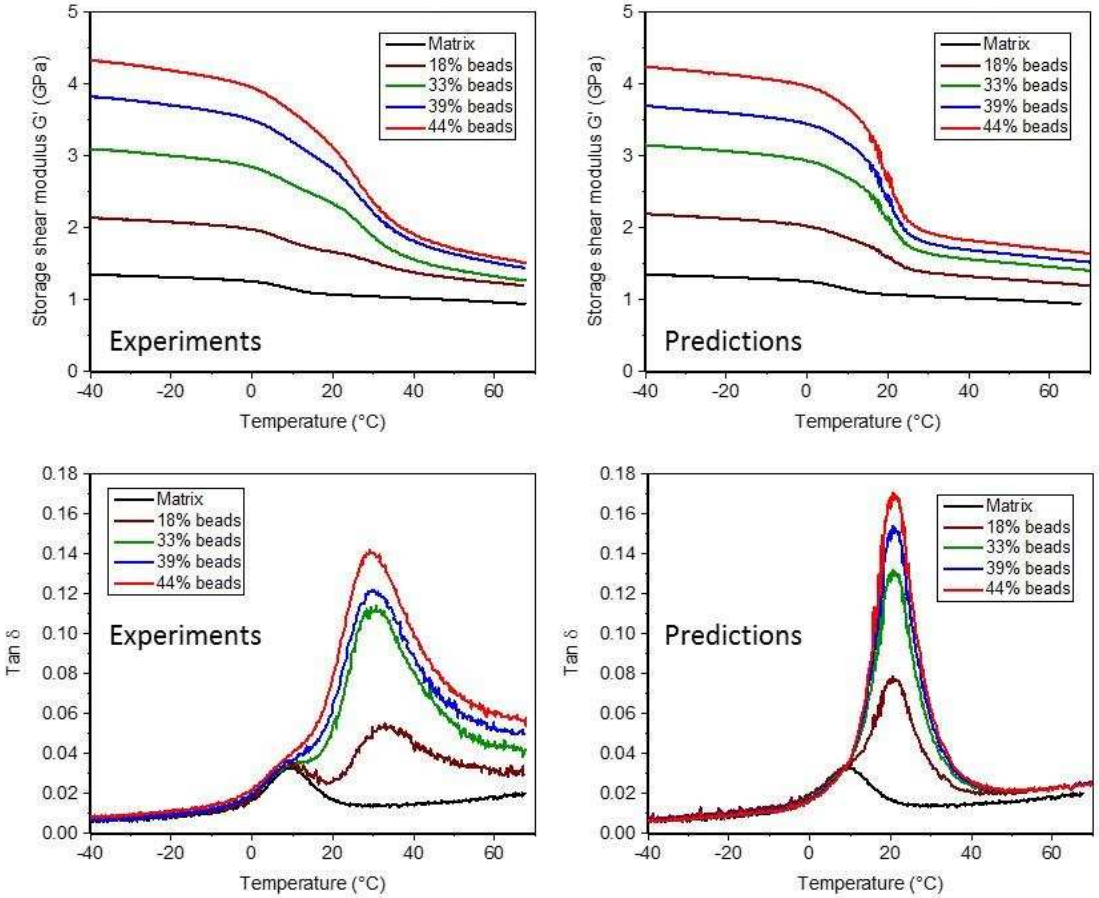


Figure 7: A comparison of the experimentally measured (Experiments), and numerically predicted (Predictions), storage modulus (G') and tan δ versus temperature for the same fractions of Barium titanate glass beads in a PS/SIS (high Tg) 90/10 blend.

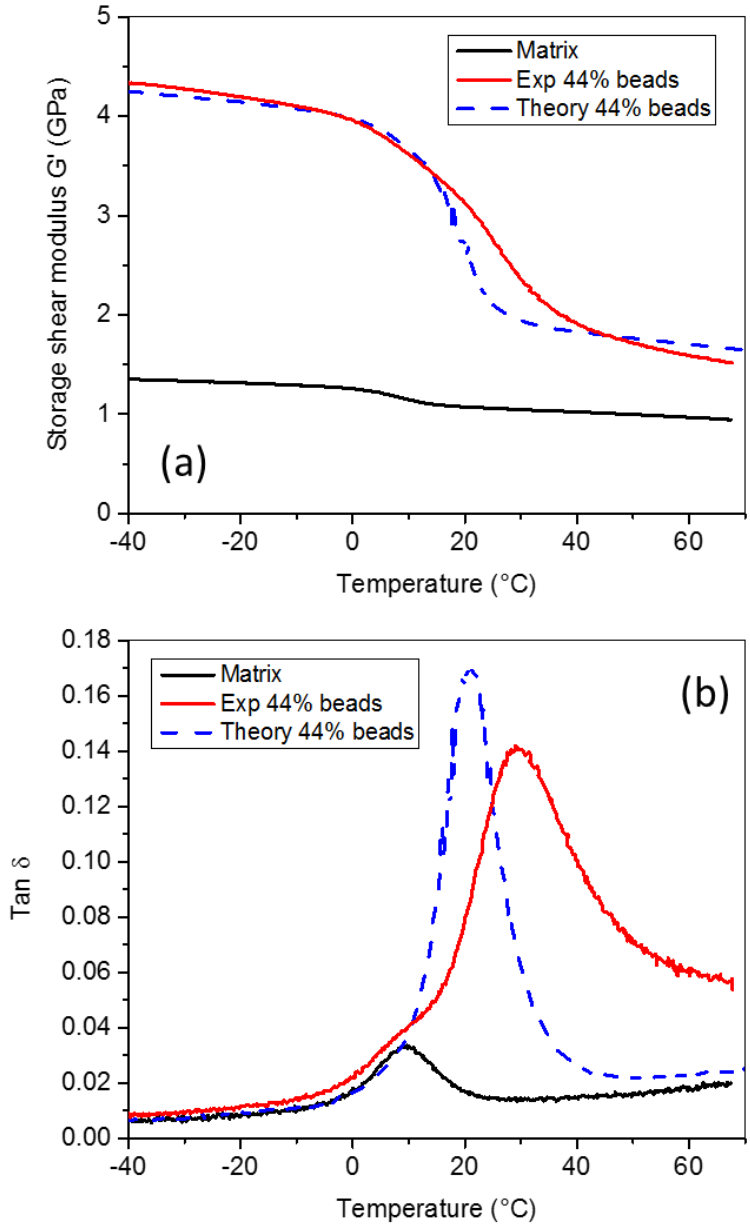


Figure 8: A comparison of the experimentally measured and numerically predicted storage modulus (G') and tan δ for 44% of Barium titanate glass beads in a PS/SIS (high Tg) 90/10 blend.

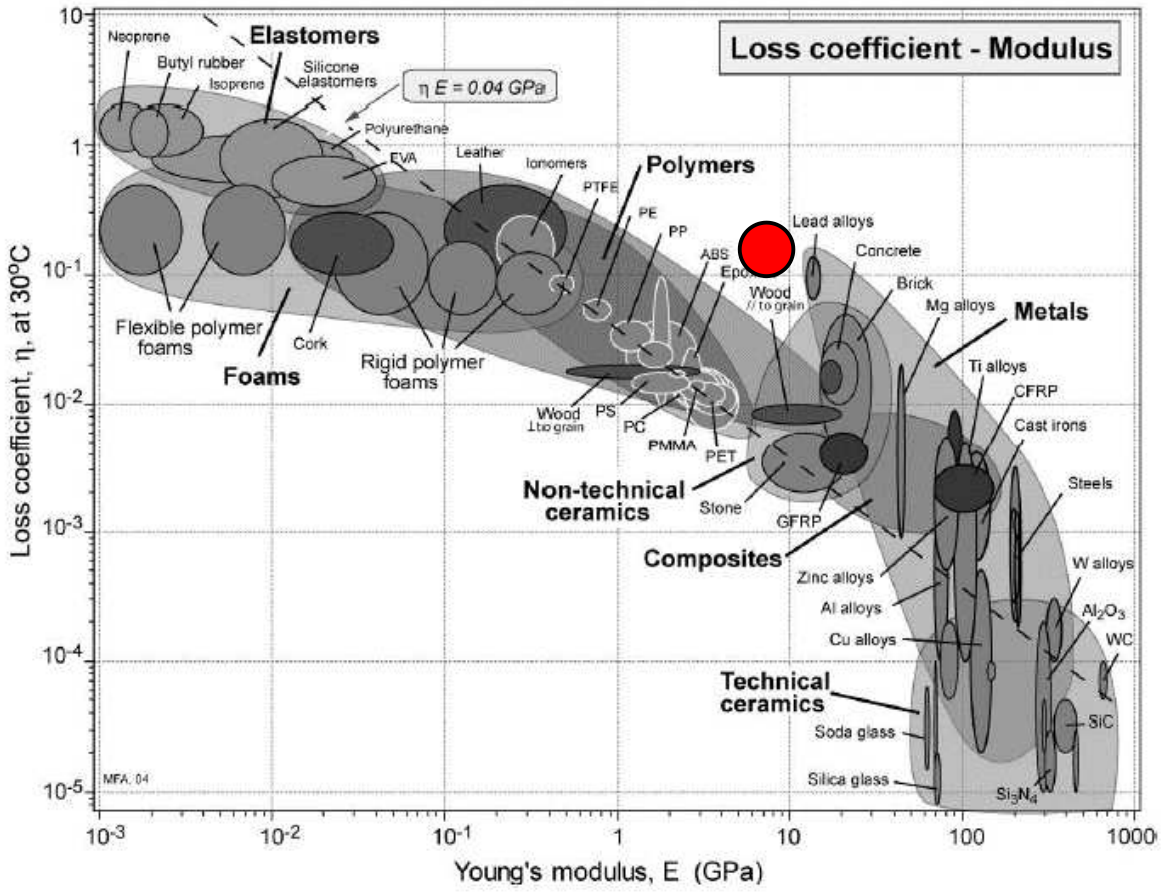


Figure 9: An Ashby log-log plot for loss coefficient η (which is tanδ) versus the storage Young's modulus E including the result (red circle) from the 90/10 PS/SIS blend with 44% uncoated Barium titanate beads.

## References


[1] M. Rueppel, J. Rion, C. Dransfeld, C. Fischer, K. Masania, Damping of carbon fibre and flax fibre angle-ply composite laminates, Composites Science and Technology 146 (2017) 1-9.

[2] D.I.G. Jones, Handbook of Viscoelastic Damping, Wiley, Chichester UK, 2001.

[3] E.E. Ungar, Noise and vibration control enginnering: Principles and Applications., Wiley, Chichester, 1992.

[4] A.W. van Vuure, I. Verpoest, F.K. Ko, Sandwich-fabric panels as spacers in a constrained layer structural damping application, Composites Part B-Engineering 32(1) (2001) 11-19.

[5] M. Alvelid, M. Enelund, Modelling of constrained thin rubber layer with emphasis on damping, Journal of Sound and Vibration 300(3-5) (2007) 662-675.

[6] R.F. Kristensen, K.L. Nielsen, L.P. Mikkelsen, Numerical studies of shear damped composite beams using a constrained damping layer, Composite Structures 83(3) (2008) 304-311.

[7] E.M. Kerwin, Damping of flexural waves by a constrained viscoelastic layer, Journal of the Acoustical Society of America 31(7) (1959) 952-962.

[8] H.J. Wang, L.W. Chen, Vibration and damping analysis of annular plates with constrained damping layer treatments, Journal of Sound and Vibration 264(4) (2003) 893-910.

[9] Y.P. Lu, J.W. Killian, G.C. Everstine, Vibrations of 3 layered damped sandwich plate composites, Journal of Sound and Vibration 64(1) (1979) 63-71.

[10] N. Le Maout, E. Verron, J. Begue, On the use of discontinuous elastomer patches to optimize the damping properties of composite sandwich plates, Composite Structures 93(11) (2011) 3057-3062.

[11] A.A. Gusev, S.A. Lurie, Loss Amplification Effect in Multiphase Materials with Viscoelastic Interfaces, Macromolecules 42(14) (2009) 5372-5377.
[12] A.A. Gusev, Optimum microstructural design of coated sphere filled viscoelastic composites for structural noise and vibration damping applications, International Journal of Solids and Structures 128 (2017) 1-10.
[13] A.P. Unwin, P.J. Hine, I.M. Ward, M. Fujita, E. Tanaka, A.A. Gusev, Escaping the Ashby limit for mechanical damping/stiffness trade-off using a constrained high internal friction interfacial layer, Scientific Reports 8(1) (2018) 2454.
[14] D.R. Paul, and Bucknall, C.B., , Polymer Blends, Wiley, Chichester, 2000.
[15] J.A. Manson, Polymer Blends and Composites, Plenum Press, New York, 1976.
[16] A.P. Unwin, P.J. Hine, I.M. Ward, O.A. Guseva, T. Schweizer, M. Fujita, E. Tanaka, A.A. Gusev, Predicting the visco-elastic properties of polystyrene/SIS composite blends using simple analytical micromechanics models, Composites Science and Technology 142 (2017) 302-310.
[17] M. Matsuo, T. Ueno, H. Horino, S. Chujyo, H. Asai, Fine structures and physical proeprties of styrene - butadiene block copolymers, Polymer 9(8) (1968) 425-436.
[18] E. Herve, A. Zaoui, N-layered inclusion-based micromechanical modelling, International Journal of Engineering Science 31(1) (1993) 1-10.
[19] R.M. Christensen, K.H. Lo, Solutions for effective shear properties in 3 phase sphere and cyclinder models, Journal of the Mechanics and Physics of Solids 27(4) (1979) 315-330.
[20] A.E.H. Love, A Treatise on the Mathematical Theory of Elasticity 2nd ed., The University Press, Cambridge, 1906.
[21] J. Goodier, Concentration of Stress around spherical and cyclidircal inclusions and flows, Journal of Applied Mechanics 55 (1933) 39-44.
[22] V.A. Matonis, Interfacial stresses in particulate composite systems, Polymer Engineering and Science 9(2) (1969) 100-&.
[23] T.T. Wang, Schonhor.H, Tensile properties of polymer-filler composites, Journal of Applied Physics 40(13) (1969) 5131-&.
[24] Z. Hashin, Complex modulii of viscoealstic composites - I. General theoryand application to particulate composites, International Journal of Solids and Structures 6 (1970) 539-552.
[25] R.M. Christensen, Theory of Viscoelasticity, 2nd ed., Academic Press, New York, 1982.
[26] A.C. Dent, C.R. Bowen, R. Stevens, M.G. Cain, M. Stewart, Effective elastic properties for unpoled barium titanate, Journal of the European Ceramic Society 27(13-15) (2007) 3739-3743.
[27] J.E. McKinney, H.V. Belcher, Dynamic compressibility of poly(vinyl acetate) and its relation to free volume, Journal of Research of the National Bureau of Standards Section a-Physics and Chemistry A 67(1) (1963) 43-45.
[28] A.A. Gusev, Finite element estimates of viscoelastic stiffness of short glass fiber reinforced composites, Composite Structures 171 (2017) 53-62.
[29] M.F. Ashby, Materials Selection in Mechanical Design Journal of Metals 40(7) (1988) A1-A2.
[30] M.F. Ashby, Materials Selection in Mechanical Design (4th Edition) - The Loss Coefficient-Modulus Chart, Elsevier1988.
[31] A.A. Gusev, P.J. Hine, A.P. Unwin, I.M. Ward, M. Fujita, E. Tanaka, 2017, Composite material and method for improving damping property thereof, WO 2017/094266 A1 (PCT/JP2016/005042), Publication Date 8th June 2017.